The coefficient of restitution for air bubbles colliding against solid walls in viscous liquids

Roberto Zenit[1] and Dominique Legendre[2]
[1]*Instituto de Investigaciones en Materiales, Universidad Nacional Autónoma de México, Apdo. Postal 70-360, México Distrito Federal 04510, Mexico*
[2]*Institut de Mécanique des Fluides de Toulouse, 1 Allée du Professeur Camille Soula, 31400 Toulouse, France*

(Received 13 February 2009; accepted 30 July 2009; published online 20 August 2009)

The motion of air bubbles undergoing collisions with solid walls was studied experimentally. Using a high speed camera, the processes of approach, contact, and rebound were recorded for a wide range of fluid properties. The process is characterized considering a modified Stokes number, $\mathrm{St}^* = (C_{\mathrm{AM}}\rho d_{\mathrm{eq}} U_0)/(9\mu)$, which compares the inertia associated with the bubble (added mass) and viscous dissipation. We found that the dependence of the coefficient of restitution, $\epsilon = -U_{\mathrm{reb}}/U_0$, with the impact Stokes number can be approximated by $-\log \epsilon \sim (\mathrm{Ca}/\mathrm{St}^*)^{1/2}$, where Ca is the capillary number; this behavior is very different from that found for the case of solid spheres. Most importantly, it shows that ϵ does not depend on the approach velocity. Considering a model for the process of contact and rebound of a deformable particle, this dependence is validated. Furthermore, by comparing the experimental trajectories and velocities of the bubble approach with model predictions, it was found that the film drainage is dominated by inertial effects; viscous effects, which would dominate for the case of approaching solid particles, are of secondary importance in this case. © *2009 American Institute of Physics*. [DOI: 10.1063/1.3210764]

I. INTRODUCTION

Particulate two-phase flows are common in many practical engineering applications, such as reactors, mineral processing, and oil extraction. Although a full comprehension of such flows is far from complete, many studies have been conducted for motion of single isolated particles;[1] a good understanding of the phenomena has been achieved. On the other hand, when particles interact with each other and with walls, not as many studies have been conducted and, therefore, the phenomena are less understood. Particularly, contact of particles (fluid or solid) is relevant in many applications and in some cases these interactions have a significant effect in the global behavior of the mixture. For instance, the collision of solid particles determines the rate of erosion in the transport of solid-liquid mixtures;[2] in flotation processes, the contact of bubbles with particles is a necessary condition.[3]

For the case of solid particles, the collision-rebound process is characterized through a lumped parameter: the coefficient of restitution, ϵ. This number is defined as

$$\epsilon = -\frac{U_{\mathrm{depart}}}{U_0}, \tag{1}$$

where U_{depart} is the velocity at which the particle loses contact with the wall and U_0 is the velocity far from the wall. It is an indirect measure of the energy dissipation that results from the contact. In numerical simulations, for instance, the coefficient of restitution can be used to simplify the particle contact process and, hence, reduce the computational load.[4] For collisions in air, the effect of the interstitial fluid can be practically neglected;[5] the energy dissipated results from plastic deformation. For particles colliding against a wall immersed in a viscous liquid, Joseph *et al.*[6] and Gondret *et al.*[7] clearly demonstrated that the coefficient of restitution can be scaled by a particle Stokes number St, which compares particle inertia to viscous effects. For collisions with a large Stokes number, the coefficient of restitution approached the value found in a dry collision. The coefficient of restitution decreases monotonically with Stokes number as viscous effects gain importance. For collisions for Stokes number below 10, approximately, the particles do not rebound but arrest against the wall ($\epsilon = 0$). Recently, Yang and Hunt[8] found that the same behavior is observed for particle-particle collisions.

Legendre *et al.*[9] showed that the concept of coefficient of restitution could also be used to characterize the collision of droplets. They argued that the coefficient of restitution could be scaled with a modified Stokes number (which accounted for the inertia of the associated fluid surrounding the droplet) in a similar manner to that observed for solid particles. Legendre *et al.*[10] reported that if the fluid inertia was also considered in the definition of Stokes number for solid particles, then the coefficient of restitution for both contaminated droplets and particles had the same universal dependence

$$\epsilon = \epsilon_{\mathrm{dry}} \exp\left(\frac{-\beta}{\mathrm{St}^*}\right), \tag{2}$$

where ϵ_{dry} is the dry coefficient of restitution and β is a constant. The modified Stokes number St^* is defined as

$$\mathrm{St}^* = \frac{(\rho_p + C_{\mathrm{AM}}\rho) d_{\mathrm{eq}} U_0}{9\mu}, \tag{3}$$

where ρ_p and ρ are the densities of the particle and liquid, respectively, μ is the liquid viscosity, $C_{\mathrm{AM}}(\chi)$ is the added

mass coefficient (which depends on the particle aspect ratio χ), d_{eq} is the particle (or droplet) equivalent diameter, and U_0 is the terminal velocity. The added mass coefficient can be calculated for any ellipsoidal shape;[11] its value increases monotonically with the aspect ratio. Defined in this manner, the Stokes number compares the total inertia available to the particle motion (associated fluid and particle) before the collision with the viscous dissipation.

One of the objectives of the study presented here is to investigate if this universal description of the coefficient of restitution found for solid spheres is also applicable for the case of air bubbles colliding against walls. We will show that, in fact, for the case of deformable particles (droplets or bubbles), the scaling of the coefficient of restitution follows a very different functional dependence.

The collision of bubbles against the walls has been studied only by a few authors. Tsao and Koch[12] studied, theoretically and experimentally, the process of collision of air bubbles in water. They reported that for a nearly spherical bubble colliding against a free interface (a large bubble) in water with salt, the coefficient of restitution was 0.85 ± 0.05 for a Stokes number (as defined here) of approximately 17. The same authors, in another study,[13] reported more detailed experiments of the collision of ellipsoidal bubbles with a horizontal wall. They, however, discussed that for the case of bubbles the "simple description" given by the coefficient of restitution was not possible because of the "finite amplitude deformation of the bubble." From their position and velocity measurements, we calculated, with the same procedure described here (below), a value of $\epsilon=0.74$ for $St^*=45$. These authors were the first to report the contact-rebound process for air bubbles in a liquid. For the case of bubbles and droplets, a rebound is possible due to the energy storage in the form of surface deformation. The balance between energy storage and viscous energy determines whether or not the bubble can rebound or not. Additionally, wall surface properties and contamination play role in determining if a rebound may occur. Malysa *et al.*,[14] Krasowska and Malysa,[15] and Zawala *et al.*[16] recently studied these aspects and their influence in the rebound of bubbles against solid walls. They have not explicitly evaluated the coefficient of restitution but it can be inferred from their raw data ($\epsilon \approx 0.85$ for a Stokes number of 49). To our knowledge, a careful parametric study of the influence of the Stokes number in the collision of air bubbles against solid walls does not exist.

Quéré and co-workers[17,18] extensively studied the bouncing of droplets for nonwetting walls. For this case, a rebound rather than a splash is possible because of the nonwetting condition allows air to be trapped at the contact point of the drop and wall. Also, since the wetting hysteresis mechanism is avoided, a large value of the coefficient of restitution was observed (approximately 0.9). Moreover, they found that, surprisingly, the contact time of colliding drops does not depend on the velocity. For such a system the Stokes number is of $O(1000)$. Hence, the dissipation does not arise from the viscosity of the surrounding fluid. They argued that the relatively low value of the coefficient of restitution was a result of shape oscillations. In our case, this effect, although possible, is not dominant because of the much smaller impact velocities attained by bubbles in viscous fluids. The same group conducted a related study for the case of bouncing soap bubbles in water.[19] For this case, the Stokes number is of $O(1)$; hence, the coefficient of restitution would be largely influenced by viscous effects. Vincent *et al.* indeed discussed that the film drainage could be significant to evaluate energy losses during the contact-rebound process. The condition of this particular experiment is closer to those presented here; however, direct comparisons are not possible since the coefficient of restitution was not reported in Ref. 19.

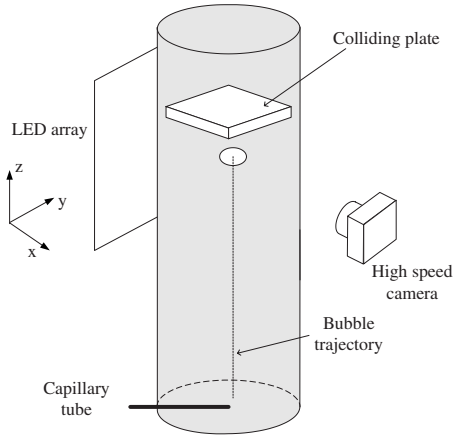

FIG. 1. Scheme of the experimental setup. $z=0$, the origin of the vertical coordinate is located at the wall.

In this paper, we report the results of an experimental investigation about the process of approach, contact, and rebound of air bubbles moving in viscous Newtonian fluids colliding against solid walls. By changing the size of the bubbles and the properties of the liquid, a wide range of conditions were tested. Hence, the transition from arrest to rebound was observed. The process of rebound is studied through the so-called coefficient of restitution, which characterizes the amount of energy loss during the contact of a body with a surface. We obtain a correlation with the Stokes and capillary numbers of the flows: such correlations show agreement with the predictions of a spring-mass-type model. To our knowledge, only few experimental results of this process exist. Nevertheless, comparisons with the existing data are also performed, leading to a good agreement.

II. EXPERIMENTAL SETUP

Experiments were performed in a glass cylindrical container with a height of 30 cm and a diameter of 10 cm, shown schematically in Fig. 1. The Plexiglas and glass walls onto which the bubbles collided were horizontal and fully immersed. The bubbles were formed with stainless steel capillaries of different diameters, which were inserted through the sidewall. The bubbles were released approximately at the center of the tube. Air gas pumped through the capillary using a syringe pump, which delivered a very small flow rate (approximately 1 μl/min), such that individual bubbles were released one at the time. All experiments were performed in room with a temperature control which kept the temperature at 22 ± 1 °C.

TABLE I. Properties of the liquids used in the experiment: ρ is the density, μ is the dynamic viscosity, and σ is the surface tension. The measured properties of water are also shown for reference.

Liquid	ρ (kg/m^3)	μ (mPa s)	σ (mN/m)	Mo$=g\mu^4/(\rho\sigma^3)$
Fluid 1	1140	4.19	65.61	9.4×10^{-9}
Fluid 2	1110	2.42	62.36	1.3×10^{-9}
Fluid 3	1080	1.96	59.80	6.3×10^{-10}
Fluid 4	1070	1.49	58.05	2.3×10^{-10}
Water	1005	1.00	69.96	2.9×10^{-11}

To vary the range of experimental conditions, both the size of the bubbles and the liquid properties were varied. The properties of a few water-glycerin mixtures used in this study are listed in Table I. The viscosity, density, and surface tension of the test liquids were measured using a stress-controlled rheometer (TA Instruments), a pycnometer (Simax, 50 ml), and Wilhelmy balance with a DuNouy ring (Sigma 700), respectively. For all the liquids used here the contact angle was approximately $30.5\pm2°$, measured on sessile bubbles resting on the wall for a long time (few minutes). For all the experiments the Morton number ranged from 7.0×10^{-10} to 2.3×10^{-7}. The bubble size was varied by using capillary tubes with different inner diameters, ranging from 0.1 to 1 mm. The Reynolds (Re$=\rho d_{eq}U_0/\mu$) and Weber (We$=\rho d_{eq}U_0^2/\sigma$) numbers ranged from 4.0 to 541.7 and from 0.02 to 3.52, respectively.

Since the main objective of this study is to investigate the collision and rebound process of bubbles, a high speed camera (APX Photron) was used. For most tests a recording rate of 3000 frames/s was used. The images were obtained at approximately 12 cm above the injection point. The bubbles were illuminated from the back using a light emitting diode array which served as a diffuse light source. Using standard image processing routines (from MATLAB©), the bubble "blob" was identified and its geometrical center was located and tracked in time to calculate the vertical velocity using a central difference scheme. The resolution of the array, considering the lenses and the camera, was of the order of 50 pixels/mm for all the experiments. The uncertainty in the measurement of the velocity considering this particle-tracking scheme is within 1.5%.

Before the analysis of the collision, the "terminal" properties of the bubbles were determined: terminal velocity, U_0, the bubble equivalent diameter [$d_{eq}=(d_l^2d_s)^{1/3}$, where d_l and d_s are the long and short bubble axes, respectively] and the aspect ratio ($\chi_0=d_l/d_s$). Most tests were performed for bubbles ascending in a straight trajectory. As is well known, when the size an air bubble in a liquid is larger than a certain critical value, its trajectory becomes oscillatory[20] because the wake loses its axisymmetry and steady nature. With the current setup it was not possible to measure the shape and trajectory of a bubble ascending in an oscillatory manner; hence, most results shown here correspond to bubbles ascending straightly. Furthermore, the rebound of a zigzagging bubble is, most likely, affected by the unsteady nature of the wake. Such effect complicates the interpretation of the measurements for such conditions. Its analysis is beyond the scope of the present communication.

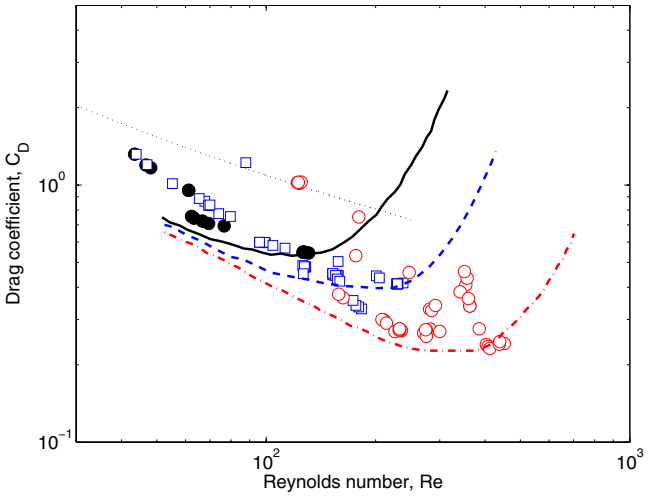

FIG. 2. (Color online) The measured drag coefficient as a function of Reynolds number for all the experiments. Different symbols show experimental ranges of Morton number: ●, $1\times10^{-7}<$Mo$<1\times10^{-8}$; □, $1\times10^{-8}<$Mo$<1\times10^{-9}$; and ○, $1\times10^{-9}<$Mo$<1\times10^{-10}$. The prediction from the theory of Moore (Ref. 21) is shown for three different liquids: solid line, Mo$=1\times10^{-8}$; dashed line: Mo$=1\times10^{-9}$; dash-dotted line: Mo$=1\times10^{-10}$. The dotted line shows the Shiller–Nauman drag correlation (Ref. 22).

The drag coefficient can be inferred indirectly from the measurements of the terminal velocity and bubble size. Assuming a steady balance between drag and buoyancy, we have

$$C_D=\frac{4}{3}\frac{gd_{eq}}{U_0^2}, \tag{4}$$

where g is the gravitational acceleration, d_{eq} is the bubble equivalent diameter, and U_0 is the terminal velocity. Figure 2 shows the drag coefficient as a function of the Reynolds number for all the experiments performed in this investigation.

Along with the experimental results, the predictions of the drag coefficient for perfectly clean ellipsoidal bubbles by Moore[21] are presented for three liquids (three values of the Morton number) with properties similar to those used in this study. Also shown in the figure is the correlation from Shiller and Nauman,[22] which is valid for solid spheres. The measured values of the drag coefficient are bounded in between the prediction for clean bubbles and that for solid spheres. In general, the experimental drag is closer (but larger) to the theoretical prediction for clean ellipsoidal bubbles. Since previous investigations have shown good agreement between experiments and the prediction of Moore for the case of bubbles in pure liquids (clean interface),[23,24] we can say that the surface of the bubbles in these experiments is not clean, but not fully immobilized either. Bubbles with a contaminated surface would show a drag coefficient closer to that expected for solid spheres.

As will be discussed later, a rebound occurs when some of the available kinetic energy of the bubble is stored as surface deformation and the dissipation is not too large. The surface energy stored in the bubble can be written as[17]

$$E_\sigma = \frac{8}{5}\pi\sigma d_{\rm eq}^2 \chi_0^{-1/3}\left[1-\left(\frac{\chi_0}{\chi_{\rm max}}\right)^{2/3}\right]^2, \quad (5)$$

where χ_0 and $\chi_{\rm max}$ are the aspect ratio away from the wall and at maximum deformation, respectively. The bubble kinetic energy, away from the wall, is

$$E_k = \frac{\pi}{12}(\rho_{\rm air}+\rho C_{\rm AM}) d_{\rm eq}^3 U_0^2. \quad (6)$$

Therefore, the ratio of these two quantities would give an idea of the energy transfer during the contact process

$$\frac{E_\sigma}{E_k} = \frac{96}{5}\frac{\chi_0^{-1/3}}{\rm We^*}\left[1-\left(\frac{\chi_0}{\chi_{\rm max}}\right)^{2/3}\right]^2, \quad (7)$$

where $\rm We^* = d_{eq} 8(\rho_{air}+\rho C_{AM}) U_0^2/\sigma$ is a modified Weber number. One would expect this ratio to be close to, but smaller than, 1 for colliding bubbles. Since all these quantities can be obtained from the image analysis of the experiments, the ratio E_σ/E_k will be calculated and discussed throughout the paper.

III. RESULTS

A. Description of the collision process

The process of approach, contact, and rebound was studied in detail for a wide range of parameters. We found that for bubbles colliding against this type of walls (hydrophobic), either bounce or arrest was observed, depending on whether the inertia or dissipation dominated the process. A typical experiment for the case of a bouncing bubble is shown in Fig. 3. It shows a sequence of images of the bubble for different instants before, during, and after the collision. Note that although the frame rate for this particular experiment was 3000 frames/s ($\Delta t = 0.33$ ms), not all images are shown. A selection has been chosen to describe the process. The time is shown in dimensionless terms: $t^* = tU_0/d_{\rm eq}$. The time origin ($t^*=0$) was chosen to coincide with the instant in which the velocity of the bubble is zero.

Along with the images, Fig. 4 shows the measurements of position, velocity, and shape of the bubble for the case shown in Fig. 3. For times $t^* < -1$, the bubble approaches the wall at its terminal speed, U_0, and shape, χ_0. During the period $-1 < t^* < -0.6$, the bubble begins to decelerate preserving its terminal shape. For $t^* \approx -0.6$, the bubble center is at approximately one diameter away from the wall. From this moment and on, the shape of the bubble begins to change importantly; the leading edge of the bubble becomes progressively flatter. From $t^* \approx -0.1$ a film between the bubble surface and the wall forms. This film thins as time progresses but does not break. For this type of wall[15] and for such large Weber numbers,[13] the wetting film does not rupture. During this period, the contact time, the bubble does not actually make "contact" with the wall and velocity decreases rapidly, reaching a value of zero. At this moment, all the kinetic energy of the bubble is transferred into deformation and dissipation such that the bubble shape reaches its maximum deformation. For this particular case, the ratio $E_\sigma/E_k = 0.51$, which shows that a significant part of the initial kinetic energy is transferred to surface deformation.

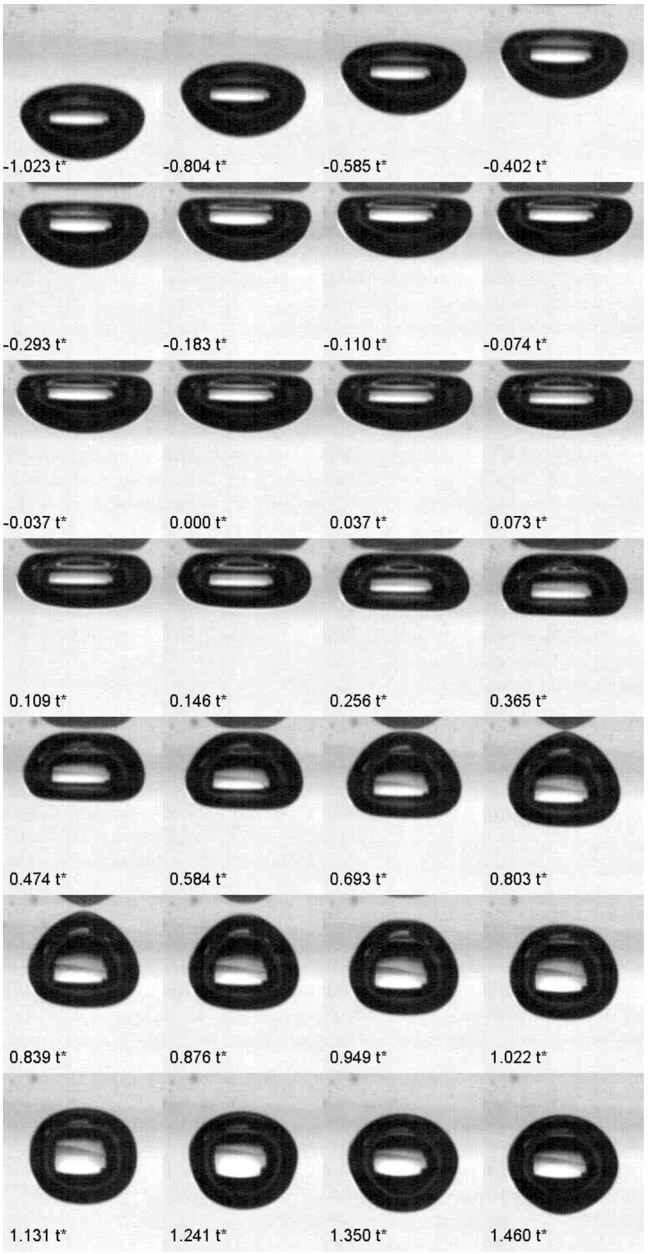

FIG. 3. Images of typical bubble collision. For the case shown, $d_{\rm eq} = 2.62$ mm, $\chi_0 = 1.63$, and $U_0 = 28.71$ cm/s, which correspond to a Re $= 214$ and We $= 3.37$ for a liquid with Mo $= 5.7 \times 10^{-9}$. For this case, $E_\sigma/E_k = 0.51$. The time stamp in the lower left corner of each image is in terms of $t^* = tU_0/d_{\rm eq}$.

After this instant, the restitution process begins ($t^* > 0$): the bubble begins to "spring back;" as the bubble moves backward the front edge flattens (before, this side was rounded). The radius of the draining film begins to reduce. The bubble appears to remain "attached" to the wall; a cusped tail forms. The tail remains in contact with the wall until $t^* \approx 0.8$. This cusp forms as the bubble surface deforms: the center of mass of the bubble is already moving away from the wall but the pressure in the film is now low, as the fluid is drawn toward the center; the film thickens first at the edges, eventually reaching the center. For the case shown, the maximum rebound velocity occurs when the cusp tail of the bubble leaves the wall. We consider that the bubble sur-

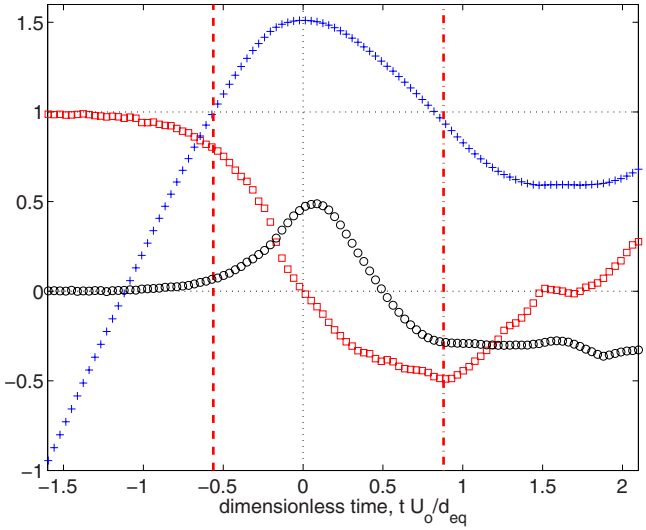

FIG. 4. (Color online) Typical bubble collision. The measurements correspond to the images shown in Fig. 3. (+), bubble position, $2z/d_{eq}+2$; (□), normalized velocity, U/U_0; and (○), normalized deformation (χ/χ_0-1). All quantities are shown as a function of the dimensionless time, $t^*=tU_0/d_{eq}$. The time $t^*=0$ corresponds to the moment for which $U/U_0=0$; positive and negative times correspond to instants after and before the zero-velocity instant, respectively. The dashed vertical line shows the time at which the bubble center is at a distance of one d_{eq} from the wall (contact time), $t^*\approx -0.6$. The vertical dashed-dotted line shows the time at which the bubble loses contact with the wall (departure time), $t^*\approx 0.8$.

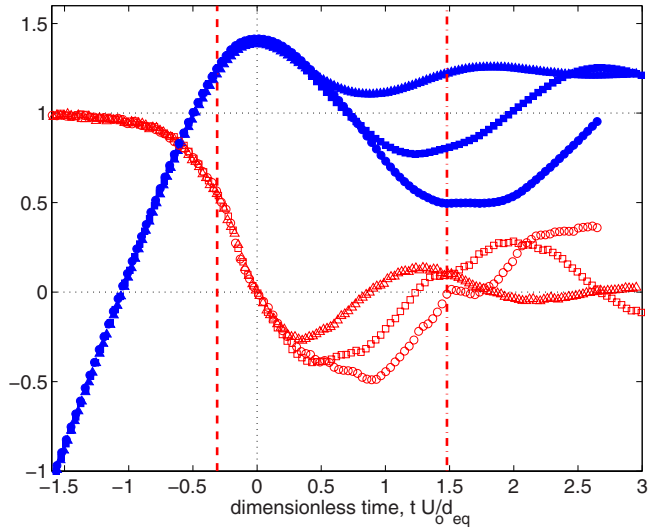

FIG. 5. (Color online) Bubble position, $2z/d_{eq}+2$, and normalized velocity, U/U_0, as a function of the dimensionless time, $t^*=tU_0/d_{eq}$. Comparison of three bubble collisions at different Stokes numbers. The filled and empty symbols denote position $(2z/d_{eq}+2)$ and velocity (U/U_0), respectively. (▲) and (△), $St^*=3.9$, $E_\sigma/E_k=0.66$, $\epsilon=0$; (■) and (□), $St^*=10.8$, $E_\sigma/E_k=0.67$, $\epsilon=0.39$; (●) and (○), $St^*=21.1$, $E_\sigma/E_k=0.51$, $\epsilon=0.54$.

face has lost contact with the wall when the distance between the bubble surface and the wall is larger than 0.04 mm, which is slightly larger than measurement resolution.

For subsequent times ($t^*>0.8$), the bubble recuperates a more round shape as its velocity progressively is reduced. At $t^*\approx 1.5$ the bubble velocity is zero again. Subsequently, the bubble moves again toward the wall and it may rebound again or simply arrest against it.

The process described above is approximately the same for bubbles for which the associated inertia is larger that the viscous dissipation; hence, some energy is stored as surface deformation and the bubble can rebound from the wall. Figure 5 shows a comparison of three experiments performed at different conditions; Fig. 6 shows the images of the same experiments at three instants of the process (terminal, zero velocity, and maximum rebound velocity). The collisions are characterized by a modified Stokes number, St^*, defined in Eq. (3). The added mass coefficient, C_{AM}, is calculated by[11]

$$C_{AM}(\chi)=\frac{(\chi^2-1)^{1/2}-\cos^{-1}\chi^{-1}}{\cos^{-1}\chi^{-1}-(\chi^2-1)^{1/2}\chi^{-2}}, \tag{8}$$

where χ is the bubble aspect ratio. Note that if $\chi=1$, the expression above recovers the well-known value of 0.5 for a sphere.

In these figures, experiments for three distinct Stokes numbers are presented. The case with smaller Stokes number ($St^*=3.9$) shows an experiment for which the bubble did not rebound from the wall. Note, however, that a negative velocity is observed after $t^*=0$. Although the bubble center moves away from the wall (due to shape oscillation), its surface remains in contact with the wall. For the other two cases shown in the figure (one of which corresponds to the case shown in Figs. 3 and 4), the bubbles do leave the wall with a finite velocity. As it will be discussed below, the rebound velocity increases as the Stokes number increases. Another interesting observation is the fact that the approach process of all bubbles is similar when presented in dimensionless form. The same amount of velocity decay prior to $t^*=0$ is observed regardless of the Stokes number. On the other hand, the rebound process is strongly dependent on the Stokes number.

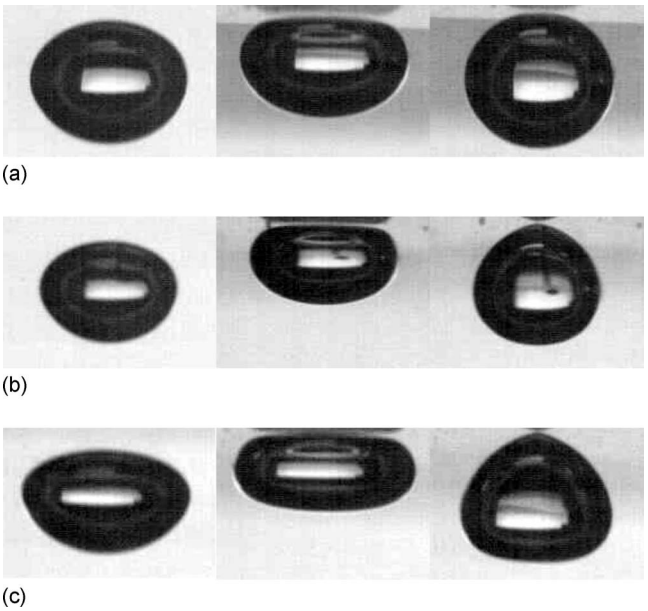

FIG. 6. Images of the bubbles at three instants: left, terminal shape ($t^*<-1$); center, maximum deformation ($t^*=0$); and right, maximum rebound velocity (or time of departure) ($t^*=t_{reb}$). The three cases correspond to those shown in Fig. 5. The scale is the same for all the images.

B. Bubble approach: Analysis of the character of the drainage

Now, we consider the drainage of the liquid between the bubble and a wall. By solving the fluid motion in the gap, the pressure field can be inferred and, hence, the hydrodynamic force can be calculated. Once the hydrodynamic force is known, a dynamic equation can be used to calculate the deceleration of the bubble as it approaches the wall. For the case of solid particles approaching a solid wall, both Joseph *et al.*[6] and Gondret *et al.*[7] showed that the film drainage satisfied the viscous approximation proposed by Davis *et al.*[25] In our case, it is interesting to note that the velocity of approach, in dimensionless form, is independent of the Stokes number, as shown in Fig. 5. This fact is in direct contradiction to what is expected for solid particles, for which the Stokes number affects directly the deceleration of the particle during the approach. Hence, we can argue that in the case of a bubble the inertial effects in the film may be important. To investigate this behavior, we conducted an analysis of the film drainage considering both a viscous and inertial flows. For the case of inertial draining, we followed closely the analysis of Weinbaum *et al.*;[26] we modified the boundary conditions to satisfy those in our problem. To calculate the viscous draining, the analysis of Davis *et al.*[25] was followed, with a minor correction to account for the nonspherical bubble shape. Details of the analysis are shown in the Appendix and in the original references.

In the limit of infinite Reynolds number, the boundary layers on the bubble and wall surfaces are vanishingly thin and viscous effects are negligible. From Eq. (A13), the evolution of the bubble velocity as it approaches the wall is

$$\frac{h_t}{U_0} = \left(\frac{2\beta+1}{2\beta+h_0/h}\right)^{3/2}, \tag{9}$$

where h is the distance from the bubble surface to the wall $[h_0=h(t=0)]$, h_t is the time rate of change of h, and

$$\beta \approx \frac{64 C_{\mathrm{AM}} m_f}{\pi \rho d_{\mathrm{eq}}^3} = \frac{32}{3} C_{\mathrm{AM}} \tag{10}$$

considering that $h_0=d_{\mathrm{eq}}$ and $L=d_{\mathrm{eq}}/2$. In our case, $\beta=O(10)$. The distance h as a function of time has to be obtained numerically. In Fig. 7 the solution of Eq. (9) is shown for a range of values of β considering that $h_0=d_{\mathrm{eq}}$.

Now, if the flow in the film is assumed to be dominated by viscous effects, then the bubble velocity can be calculated to be [Eq. (A28)]

$$\frac{h_t}{U_0} = 1 - \frac{1}{\Pi}\ln\frac{h_0}{h}, \tag{11}$$

where Π is defined as

$$\Pi = \frac{2(m_{\mathrm{air}} + C_{\mathrm{AM}} m_f) U_0}{3\mu\pi b^2 \chi^2} = 4\chi^{-4/3}\ \mathrm{St}^*. \tag{12}$$

The distance h is then given by

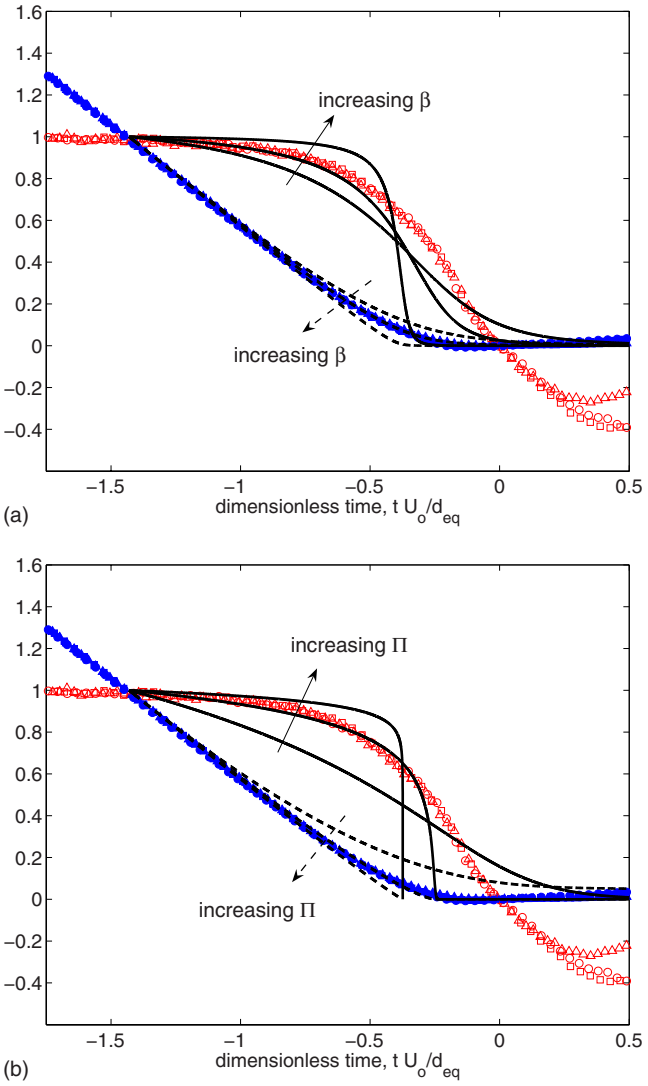

FIG. 7. (Color online) (a) and (b) show the comparison between experiments and the inertial [Eq. (9)] and viscous [Eq. (11)] drainage predictions, respectively. The solid lines show h_t and the dashed lines h. The different lines show predictions for varying β or Π: (a) $\beta=5,10,50$ (b) $\Pi=3,8,20$, which correspond approximately to $\mathrm{St}^*=0.9,2.2,5.6$. The filled and empty symbols denote experimental results of (h/d_{eq}) and (U/U_0), respectively; the results here correspond to those shown in Fig. 4.

$$\Pi e^{-\Pi}\left[Ei(\Pi) - Ei\left(\Pi - \ln\frac{h_0}{h}\right)\right] = \frac{U_0 t}{d_{\mathrm{eq}}}, \tag{13}$$

where Ei is the exponential integral function.

In Fig. 7, the predictions of the inertial and viscous drainage models are compared and contrasted with experimental measurements. The distance h is calculated from the experiments as

$$h = z - \tfrac{1}{2} d_{\mathrm{eq}} \chi^{-2/3},$$

where z is the distance from the bubble center to the wall. The three experiments shown in the figure are the same as those in Fig. 4.

The comparison shows that the inertial drainage mechanism fits the experimental results more closely. In particular, the model prediction is close to the experimental measurements at a distance not very near to the wall. It is expected

that when the gap is very thin, the viscous effects cannot be neglected. Furthermore, the behavior of the prediction depends on the parameter β, which remains $O(10)$ and in a narrow range for all the experiments ($11.8 < \beta < 15.3$, for the three experiments shown in Fig. 5). The prediction does not change significantly for these range of values of β and is close to the experimental observations. On the other hand, the prediction from the viscous draining model can be made to coincide the experimental observations but only for a particular value of the Stokes number, which is in fact lower that the corresponding value in the experiments ($St^* \approx 2.2$). Moreover, in the experiments, the value of St^* varies significantly (in the data shown in Fig. 7, it varies from 4 to 20); the corresponding curves for such values of St^* are very different from each other. Therefore, we can conclude that the dominating mechanism for film drainage, and the associated hydrodynamic force, before contact is the inertia of the fluid. The viscous effects are only important when the film is very thin.

C. Coefficient of restitution

As discussed in Sec. I, for solid particles[6,7] and liquid drops,[9] the Stokes number correctly characterizes the collision process. The restitution coefficient "lumps" the process into a single parameter. For the case of bubble collisions, we define this parameter as the negative of the ratio between rebound and incoming velocity

$$\epsilon = -\frac{U_{\text{depart}}}{U_0}, \tag{14}$$

where U_{depart} is the velocity at which the bubble loses contact with the wall and U_0 is the bubble terminal velocity. Defined in this manner, the coefficient of restitution gives a global description of the energy dissipation during the approach, contact, and bounce. Legendre *et al.*[9] discussed that the coefficient of restitution could be defined in different manners, depending on the value chosen for the approach velocity (either the contact or terminal velocity). In our case, we opted for the definition shown above because of the difficulty of accurately determining the point in which the bubble effectively contacts the wall.

Figure 8 shows the measured coefficient of restitution ϵ as a function of the Stokes number for all the experiments performed in this investigation. The coefficient of restitution is observed to decrease monotonically with Stokes. This is an indication of the two competing mechanisms in the process: viscous dissipation and the inertia associated with the collision. When the Stokes number is small, viscous dissipation dominates over inertia and the bubble motion is damped before a rebound can occur. On the other hand, when the inertia is sufficient, the bubble reaches the wall with enough energy to overcome dissipation and store it in the form of surface deformation. The surface deformation energy is recovered into kinetic energy and bubble bounces off the wall with a velocity smaller that the incoming one. Note also that no difference in behavior was found when bubbles collided against a glass or Plexiglas wall. In the figure, we also present the values of the coefficient of restitution inferred from Tsao and Koch[13] and Malysa *et al.*[14] Although these previous data are limited, good agreement is found. The measurements for oscillating bubbles appear to have slightly higher values of the restitution coefficient; however, a more in depth analysis for oscillating bubbles was not pursued.

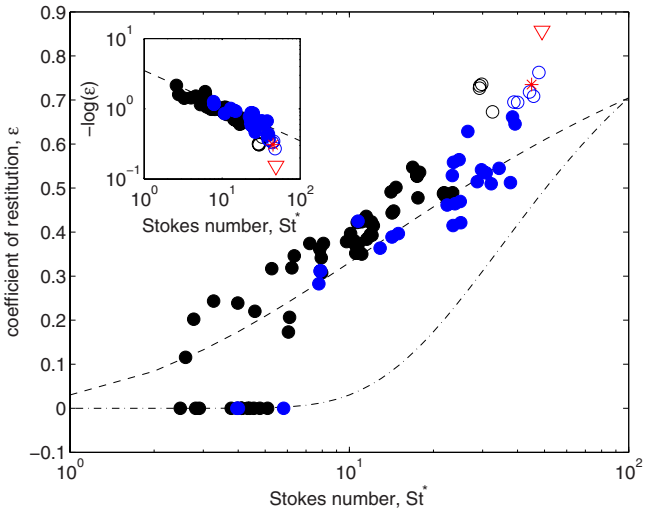

FIG. 8. (Color online) Coefficient of restitution ϵ as a function of Stokes number St^*. The solid and empty circles show the results obtained for bubbles rising in a straight and oscillatory path, respectively. The blue and black circles show the results obtained for bubbles colliding against a glass and Plexiglas wall, respectively. The dashed and dashed-dotted lines correspond to expressions (15) and (16), respectively. Results from others: Tsao and Koch (Ref. 13) (∗); Malysa *et al.* (Ref. 14) (▽). The inset shows $-\log(\epsilon)$ as a function of the Stokes number.

From the figure it can also be noted that, although the trend is very clear, a certain amount of scatter is present. In addition to the uncertainty from the experimental technique, we believe that the fact that our experiments are conducted under ordinary laboratory conditions (not an ultrapure environment) causes some additional variability of the results. The terminal conditions of an approaching bubble may vary depending on how much contamination is contained on its surface. Also, for the same approach conditions, the rebound velocity may change depending on the degree of contamination that the bubble surface acquires during the contact with the wall. These effects, which cannot be quantified, result in the dispersion of the experimental results, which can be as high as 20%.

For the same reason, it is not possible to accurately determine the value of the Stokes number for which the transition from bounce to arrest occurs. We observed that for the same nominal conditions, sometimes rebound or arrest could be observed. Surface active agents, possible present in our arrangement, wall wettability, and roughness[15] add additional effects that could prevent the bubble from leaving the wall. The fact that these effects may vary under the same laboratory conditions explain the variability observed in our measurements. Extrapolating our measurements, the value of the critical Stokes number would be approximately 1.

By plotting the data as $-\log(\epsilon)$ as a function of St^* (as shown in the inset in Fig. 8), we can observe that the coefficient of restitution can be closely fitted to

$$\epsilon = \exp\left(-\frac{\beta_1}{\sqrt{\mathrm{St}^*}}\right), \tag{15}$$

where $\beta_1 = 3.5$. The only data that appear not to follow this trend are that obtained from oscillating bubbles. This functional dependence is very different to that reported for the case of solid spheres and liquid drops by Legendre *et al.*[10]

$$\epsilon = \exp\left(-\frac{\beta_2}{\mathrm{St}^*}\right), \tag{16}$$

where β_2 is equal to 35. In Sec. IV we will discuss the nature of this different functional dependence for bubble collisions.

IV. SCALING OF THE COEFFICIENT OF RESTITUTION

Legendre *et al.*[9] proposed a simple model for the contact-rebound process of droplets colliding with a wall. Since we found that the functional dependence of the coefficient of restitution with the Stokes number is significantly different for bubbles and particles, it is instructive to revise the model.

The model contemplates a dynamic equation for deformation of the bubble (or droplet), valid only during the duration of contact with the wall. The deformation is written in terms of the length η (as defined in Ref. 9), which represents the difference between the instantaneous and terminal minor semiaxes of the bubble. With some minor modifications, the dynamic equation can be written as

$$m^*\frac{\partial^2\eta}{\partial t^2} + C_\mu\frac{\partial\eta}{\partial t} + C_\sigma\eta = 0, \tag{17}$$

where $m^* = (4/3)\pi R^3\rho^*$, $C_\mu = K_1\mu R$, and $C_\sigma = K_2\sigma$. Also, $\rho^* = \rho_{\mathrm{air}} + \rho C_{\mathrm{AM}}$. The second term in Eq. (17) represents the viscous dissipation; it is given by the product of the viscosity and a characteristic velocity. Legendre *et al.*[9] showed that the characteristic velocity was, in fact, the velocity of deformation. This term accounts for the viscous dissipation in the draining film and can be shown to scale with the capillary number. The third term in Eq. (17) models the energy storage (a *spring* term). It accounts for the energy stored as surface energy. Hence, one can expect the coefficient C_σ to depend on the bubble aspect ratio.

In dimensionless form, considering $\hat{\eta} = \eta/R$ and $\hat{t} = tU_0/R$, where R is the bubble equivalent radius ($2R = d_{\mathrm{eq}}$) and U_0 is the terminal velocity, and dropping the "^" symbols, Eq. (17) can be written as

$$\frac{\partial^2\eta}{\partial t^2} + \frac{\kappa_1}{\mathrm{St}^*}\frac{\partial\eta}{\partial t} + \frac{\kappa_2}{\mathrm{St}^*\ \mathrm{Ca}}\eta = 0, \tag{18}$$

where St^* is the modified Stokes number [defined in Eq. (3)] and $\mathrm{Ca} = U_0\mu/\sigma$ is the capillary number. The constants κ_1 and κ_2 have absorbed all numerical constants. Considering the initial conditions $\eta(0) = 0$ and $\partial\eta/\partial t(0) = 1$, the solution for η is

$$\eta = \frac{1}{C}\exp\left(-\frac{\kappa_1}{2\ \mathrm{St}^*}t\right)\sin(Ct), \tag{19}$$

where

$$C = \sqrt{\frac{\kappa_2}{\mathrm{St}^*\ \mathrm{Ca}}}\left|1 - \frac{\kappa_1^2}{4\kappa_2}\frac{\mathrm{Ca}}{\mathrm{St}^*}\right|^{1/2}. \tag{20}$$

Note that $\mathrm{St}^*\mathrm{Ca} = \mathrm{We}^*$, where $\mathrm{We}^* = 2R\rho^*U_0^2/\sigma$ is a modified Weber number.

We can obtain an estimation of the coefficient of restitution ϵ by considering

$$\epsilon = -\frac{\left.\frac{\partial\eta}{\partial t}\right|_{t=t_{\mathrm{reb}}}}{\left.\frac{\partial\eta}{\partial t}\right|_{t=0}} = -\left.\frac{\partial\eta}{\partial t}\right|_{t=t_{\mathrm{reb}}}. \tag{21}$$

From the experiments, t_{reb} roughly corresponds to the time at which the bubble recovers its initial deformation after the compression-decompression process ($\eta = 0$). It follows from Eq. (19), that $\eta = 0$ when

$$t_{\mathrm{reb}} = \frac{\pi}{C}. \tag{22}$$

Therefore,

$$\epsilon = \exp\left(-\frac{\pi}{2}\frac{\kappa_1}{\mathrm{St}^*}\frac{1}{C}\right). \tag{23}$$

From the value of C [Eq. (20)] and since $\kappa_1^2\ \mathrm{Ca}/(4\kappa_2\ \mathrm{St}^*)$ is small [of order $O(0.01)$ for our case], we can write

$$\epsilon \approx \exp\left(-\frac{\pi}{2}\frac{\kappa_1}{\sqrt{\kappa_2}}\sqrt{\frac{\mathrm{Ca}}{\mathrm{St}^*}}\right). \tag{24}$$

This expression, which, in fact, can be deduced from the results of Legendre *et al.*,[9] gives a functional dependence of $-\log(\epsilon) \propto \mathrm{St}^{*-1/2}$ for a given value of Ca. This is in accordance with the measurements shown in Fig. 8. Moreover, this analysis reveals that the proper dimensionless number that characterizes the collision-rebound process of bubbles and droplets is not the Stokes number alone; instead, the number $\mathrm{Ca}/\mathrm{St}^* = 9\mu^2/(2R\rho^*\sigma)$ should give the correct scaling of the problem. Note that $\sqrt{\mathrm{Ca}/\mathrm{St}^*}$ is, in fact, the so-called the Ohnesorge number, used in the spray technology literature.[27] Figure 9 shows the measured coefficient of restitution now as a function of the ratio $\mathrm{Ca}/\mathrm{St}^*$. The data clearly follow the expected functional dependence. A best fit reveals

$$\epsilon = \exp\left(-30\sqrt{\frac{\mathrm{Ca}}{\mathrm{St}^*}}\right). \tag{25}$$

Also noteworthy is the agreement with the experimental results of Tsao and Koch[13] and Malysa *et al.*,[14] as shown in the figure.

The fact that the data can be presented well either in terms of St^* (Fig. 8) or $\mathrm{Ca}/\mathrm{St}^*$ (Fig. 9) results from the fact that in the experiments performed here the capillary number does not change significantly (it ranges approximately from 0.005 to 0.02) and remains relatively constant.

A closer examination of the results of Legendre *et al.*[9] reveals that their measurements can be closely fitted to ϵ

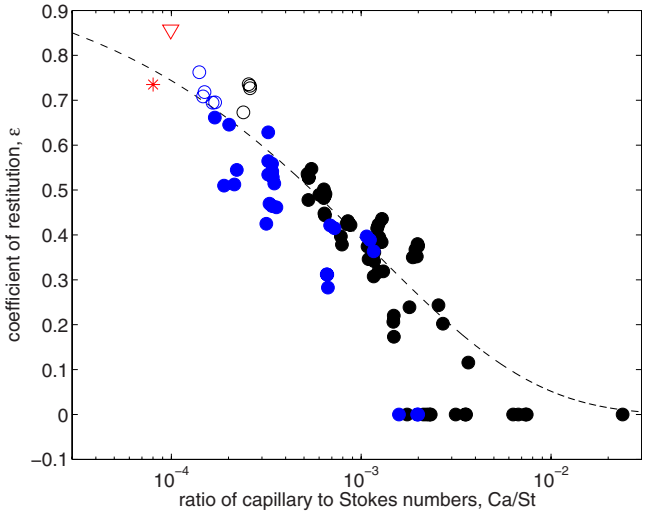

FIG. 9. (Color online) Coefficient of restitution ϵ as a function of $\mathrm{Ca}/\mathrm{St}^*$. All symbols as in Fig. 8. The dashed line corresponds to expression (25).

$=\exp(-10\sqrt{\mathrm{Ca}/\mathrm{St}^*})$, with the same functional dependence as Eq. (25). It is, in fact, difficult to discern whether $\sqrt{\mathrm{Ca}/\mathrm{St}^*}$ or 1/St is the proper dimensionless parameter, which characterizes their collision process. It must be noted that the range of parameters in their study was not large enough and also their range of Ca values was narrow. Based on the analysis presented above, we believe that the proper parameter should be $\sqrt{\mathrm{Ca}/\mathrm{St}^*}$. The dependence of the coefficient of restitution given by Legendre *et al.*($\log \epsilon \sim -1/\mathrm{St}^*$) and that inferred here ($\log \epsilon \sim -\sqrt{\mathrm{Ca}/\mathrm{St}^*}$) gave similarly good fittings, by coincidence, in their small range of experimental parameters.

Finally, it is important to note that in the relation $\sqrt{\mathrm{Ca}/\mathrm{St}^*}$ the velocity U_0 cancels out. This would imply that the coefficient of restitution would not depend on approach velocity. This result, although surprising, is expected from the fact that the model considered here is linear. The energy storage mechanism of the model is linearly proportional to deformation; hence, it is expected that $U_{\mathrm{depart}} \sim U_0$. For the case of solid spheres, this is not the case. The elastic energy is a nonlinear function of deformation[28] and therefore it is expected that the rebound velocity is not directly proportional to the approach velocity.

V. CONCLUSIONS

The process of approach-contact-rebound of air bubbles against solid walls was studied experimentally. A detailed examination of the evolution of the position, velocity, and shape of the bubble during the process was presented for a wide range of conditions.

First, we found that the bubble approach process is dominated by the inertia in the draining film between the bubble and the wall. By comparing the trajectory and velocity of the bubble, as it approaches the wall, with film draining models we found that the inertial prediction fits well with the experimental results.

The bubble-wall interaction process was found to evolve in a manner similar to that for solid particles or liquid drops: when the inertia associated with the bubble motion dominates over viscous dissipation, a rebound is observed; on the other hand, when the inertia is not enough to overcome dissipation, the bubble may oscillate or arrests over the wall, but no rebound is observed. The process is characterized with an effective coefficient of restitution, which compares the rebound and approach velocities. We found that there is a clear correlation between the coefficient of restitution and the bubble Stokes number. The functional dependence between these two parameters was found to be significantly different from that observed for the case of solid particles. Considering a simplified mass-spring-type model, the collision process was analyzed. It was found that if both surface tension and viscous effects are accounted for, the coefficient of restitution should evolve with the number $\mathrm{Ca}/\mathrm{St}^* = 9\mu^2/(2R\rho^*\sigma)$ and not only with St^*. Such dependency was in very good agreement with what was found experimentally. More experiments are necessary to further corroborate this dependence for colliding fluid particles. In particular, it would be important to obtain measurements (through experiments or numerical simulations) for systems in which Ca and St^* could be varied independently. Moreover, it is necessary to perform experiments considering clean fluids in order to obtain a precise measurement of the critical value of the Stokes number beyond which a rebound can be expected. We plan to continue our investigation in these lines in the future.

ACKNOWLEDGMENTS

These experiments were performed, in part, at the IMFT during the sabbatical year of R.Z., who acknowledges the support of the PASPA program of UNAM. The help of A. Ordoñez (†) with the surface tension measurements was greatly appreciated.

APPENDIX: FILM DRAINING AND RESULTING HYDRODYNAMIC FORCE

In this appendix we show the summary of the analysis done to obtain expressions for the bubble deceleration as a result of the hydrodynamic force on the film. We follow two approaches. First, we analyze the case in which the drainage is inertial. The equation for inertial drainage in a film was first derived by Weinbaum *et al.*[26] for the draining of a thin fluid layer between parallel plates. We use this analysis with the boundary and initial conditions related to our problem. On the other hand, we follow the analysis of Davis *et al.*[25] to calculate the viscous draining adding the effect of the oblateness of the bubble.

1. Inertial draining

Let us consider the arrangement depicted in Fig. 10: a bubble of equivalent diameter d_{eq} ascending straightly at its terminal velocity U_0, approaching a horizontal rigid wall.

Far from the wall, the evolution of the distance from the surface to the wall h is given by

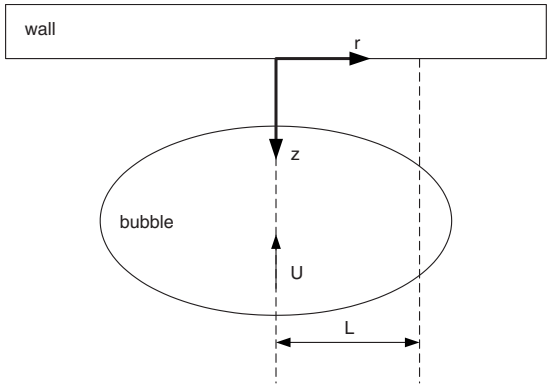

FIG. 10. Sketch of the geometry showing the coordinate axes and dimensions.

$$w = \frac{dh}{dt} = -U_0, \quad \text{i.e.,} \quad h(t) = h_0 - U_0 t, \tag{A1}$$

where by definition $-h_t = -dh/dt$ is the instantaneous velocity of the bubble. Since the bubble is deformed, we assume that at first order the lubrication occurs between two parallel plane surfaces. The bubble is considered equivalent to a disk of radius $L = O(d_{eq})$ and we assume that the fluid is at rest in front of the bubble. In fact, since $\mathrm{Re} \gg 1$, the flow decays as d_{eq}^3/r^3 (potential flow) so that the flow is at rest for $d_{eq}^3/h^3 \ll 1$. Under these conditions, we consider that the bubble sees the wall instantaneously at time $t=0$. We want to study the induced inertial drainage of the fluid between the bubble and the wall.

Weinbaum *et al.*[26] considered a two-dimensional axisymmetric flow in the gap between the bubble and the wall. They formulated the solution in terms of a stream function Ψ,

$$u = \frac{1}{r}\frac{\partial \Psi}{\partial z} = rF_z(z,t), \tag{A2}$$

$$w = -\frac{1}{r}\frac{\partial \Psi}{\partial r} = -2F(z,t), \tag{A3}$$

where u and w are the fluid velocities in the r and z directions, respectively, and $F(z,t)$ is an unknown function that can be determined by the boundary and initial conditions of the problem.

The boundary conditions at the wall, $z=0$, are $F=0$ and $F_z=0$; at the bubble surface, the normal velocity condition and the zero shear stress give $F=-h_t/2$ and $F_{zz}=0$. The initial condition is $2F=-h_t=U_0$ at $h=h_0$.

Substituting Eq. (A2) into the Navier–Stokes equations and integrating the pressure in r and z, one can obtain, after some manipulations, following Ref. 26, the pressure distribution on the bubble surface

$$p(r,h,t) = \tfrac{1}{2}\rho r^2 A(t) + p_0(t), \tag{A4}$$

where $p_0(t)$ is the pressure at the center $(r=0)$ of the lower surface of the body. The function $A(z,t)$ resulting from the integration of the pressure is

$$A(z,t) = \nu F_{zzz} - F_{zt} - F_z^2 + 2FF_{zz}. \tag{A5}$$

The unknown function $A(t)$ can be related to the instantaneous motion of the bubble. Assuming that the dominant effect is induced by the inertial drainage and considering that during the deceleration, the viscous drag balances the buoyancy, the bubble force balance can be written as

$$C_{AM} m_f h_{tt} = D(t), \tag{A6}$$

where $m_f = \pi d_{eq}^3 \rho/6$ is the mass of fluid displaced, C_{AM} is the added mass coefficient [defined in Eq. (8)], and $D(t)$ is the hydrodynamic force.

By assuming that the normal viscous stresses are of second order, the hydrodynamic force can be calculated integrating the pressure profile over the bubble surface,

$$D(t) = \int_0^L 2\pi r p(r,h,t) dr = \frac{1}{2}\pi \rho L^4 A(t). \tag{A7}$$

This expression is obtained by considering that the reference pressure is zero. Therefore, the relation between $A(t)$ and h_{tt} is

$$A(t) = -\frac{4C_M m_f}{\rho \pi L^4} h_{tt}. \tag{A8}$$

Thus, the film equation in dimensionless form (considering $z^* = z/h_0$, $h^* = h/h_0$, $F^* = F/U_0$, and $t^* = tU_0/h_0$ and dropping the asterisks) can be written as

$$F_{zt} + F_z^2 - 2FF_{zz} - \frac{1}{\mathrm{Re}_0} F_{zzz} = \beta h_{tt}, \tag{A9}$$

with the Reynolds number $\mathrm{Re}_0 = h_0 U_0 \rho/\mu$ and β given by

$$\beta = \frac{4C_M m_f h_0}{\rho \pi L^4}. \tag{A10}$$

For our case, we can consider that $h_0 \approx d_{eq}$ and that $L \approx d_{eq}/2$; hence, we have $\beta = O(10)$.

In the infinite Re limit, the boundary layers at $z=0$ and $z=h(t)$ can be assumed to be vanishingly thin $\delta \ll h_0$ and thus the viscous term in Eq. (A9) disappears. In the case of a bubble, the boundary layer thickness is $\delta \approx b\ \mathrm{Re}_0^{1/2}$; therefore, we will assume that the viscous effects in the gap are negligible. The film equation then reduces to

$$F_{zt} + F_z^2 - 2FF_{zz} = \beta h_{tt}. \tag{A11}$$

Furthermore, following Ref. 26, it can be assumed that $\Psi = r^2 z \Phi(t)$ since the flow resembles a time-dependent axisymmetric stagnation-point flow. After some algebra, an equation for the evolution of h can be obtained

$$\left(\beta + \frac{1}{2h}\right) h_{tt} - \frac{3}{4h^2} = 0 \tag{A12}$$

with the initial conditions $h_t(0) = -1$ and $h(0) = 1$.

The solution for h_t can, in fact, be obtained analytically

$$h_t = \left[\frac{h(2\beta+1)}{2\beta h + 1}\right]^{3/2}. \tag{A13}$$

The solution of h, however, has to be obtained by numerical integration. These expressions are compared with our experi-

mental results in Sec. III B. Note that for this case, obviously, the evolution of h_t with time is independent of the Stokes number of the flow since the effect of viscosity was not considered.

2. Viscous draining

We consider that the bubble is an ellipsoid of revolution along its small axis, as shown in Fig. 10. The bubble surface is perfectly clean and it is allowed to deform during the film drainage. We note h_0 the position of the ellipsoid before the deformation and λ is the deformation induced by the interaction with the wall. The instantaneous gap between the bubble and the wall is thus

$$h(r,t) = h_0 + \lambda(r,t). \tag{A14}$$

The initial shape of the bubble can be approximated by paraboloids in the region of near contact and the deformation gap profile is

$$h(r,t) = z(t) + \frac{r^2}{2b\chi} + \lambda(r,t), \tag{A15}$$

where $z(t)$ is the distance between the wall and the bubble and b is the bubble small semiaxis. We assume that the wall does not deform so that $\lambda(r,t)$ results only from the deformation of the bubble. For $\chi=1$ (spherical shape), Eq. (A15) recuperates the original result of Davis *et al.*[25] for an spherical shape.

Before the interaction with the wall, the bubble is deformed resulting from the hydrodynamic interaction with the fluid. Neglecting normal viscous stresses, the shape is given by

$$p_B - p_L = 2H\sigma \quad \text{with} \quad H = \frac{1}{r}\frac{\partial}{\partial r}\left(r\frac{\partial h}{\partial r}\right), \tag{A16}$$

with H being the mean curvature of the bubble surface. By noting $H_0=2/b\chi$ the curvature in the region of near contact, the additional deformation is related to the pressure in the film by

$$p = -\frac{\sigma}{r}\frac{\partial}{\partial r}\left(r\frac{\partial \lambda}{\partial r}\right). \tag{A17}$$

Under the lubrication assumption, the Navier–Stokes equations reduce to

$$\frac{\partial p}{\partial r} = \mu\frac{\partial^2 u}{\partial r^2}, \tag{A18}$$

$$\frac{\partial p}{\partial z} = 0, \tag{A19}$$

by integration along z the velocity profile is

$$u = \frac{1}{2\mu}\frac{dp}{dr}(z^2 - hz) + U_I\frac{z}{h}, \tag{A20}$$

where U_I is the interfacial velocity.

From the continuity equation

$$\frac{\partial h}{\partial t} = -\frac{1}{r}\frac{\partial}{\partial r}\left(r\int_0^z u dz\right), \tag{A21}$$

and combining Eqs. (A20) and (A21), one obtains

$$\frac{\partial h}{\partial t} = -\frac{1}{r}\frac{\partial}{\partial r}\left[r\left(\frac{U_I h}{2} - \frac{1}{12\mu}h^3\frac{dp}{dr}\right)\right]. \tag{A22}$$

Considering the zero-shear stress boundary condition, after some manipulations, we obtain

$$U_I = -\frac{3}{4}\frac{r}{h}z_t, \tag{A23}$$

$$p = \frac{3}{4}\mu\chi b\frac{z_t}{\left(z + \frac{r^2}{2\chi b}\right)^2}. \tag{A24}$$

Integrating the pressure over the surface, the hydrodynamic force on the bubble is

$$D(t) = \frac{3}{2}\pi\mu b^2\chi^2\frac{z_t}{z}. \tag{A25}$$

Note that Davis *et al.*[25] obtained $D(t)=6\pi\mu a^2 z_t/z$ for the case of a solid sphere.

Now, the motion of the bubble during the film drainage can be obtained by a dynamic equation given by

$$[m_{\text{air}} + C_{\text{AM}}(\chi)m_f]z_{tt} = -D(t). \tag{A26}$$

Introducing the dimensionless quantity,

$$\Pi = \frac{2(m_{\text{air}} + C_{\text{AM}}(\chi)m_f)U_0}{3\mu\pi b^2\chi^2} = 4\chi^{-4/3}\ \text{St}^*, \tag{A27}$$

where St^* is the modified Stokes number [defined in Eq. (3)], and considering the initial conditions $z_t=U_0$ and $z=z_0$, the solution of this problem resembles that obtained by Davis *et al.*[25]

$$\frac{z_t}{U_0} = 1 - \frac{1}{\Pi}\ln\frac{z_0}{z}. \tag{A28}$$

The distance between the bubble and wall, z, which can, in fact, be obtained analytically, is then given by

$$\Pi e^{-\Pi}\left[Ei(\Pi) - Ei\left(\Pi - \ln\frac{z_0}{z}\right)\right] = \frac{U_0 t}{z_0}. \tag{A29}$$

The predictions of these expressions are shown in Fig. 7, compared to the predictions of inertial draining and experiments.

[1] R. Clift, R. J. Grace, and M. E. Weber, *Bubbles, Drops and Particles* (Dover, New York, 2005).
[2] H. M. Clark, "On the impact rate and impact energy of particles in a slurry pot erosion tester," Wear **147**, 165 (1991).
[3] K. A. Matis, *Flotation Science and Engineering* (CRC, New York, 1994).
[4] K. Hadinoto and J. S. Curtis, "Effect of interstitial fluid on particle-particle interactions in kinetic theory approach of dilute turbulent fluid-particle flow," Ind. Eng. Chem. Res. **43**, 3604 (2004).
[5] S. F. Foerster, M. Y. Louge, A. H. Chang, and K. Allia, "Measurements of the collision properties of small spheres," Phys. Fluids **6**, 1108 (1994).
[6] G. G. Joseph, R. Zenit, M. L. Hunt, and A. M. Rosenwinkel, "Particle wall collision in a viscous fluid," J. Fluid Mech. **433**, 329 (2001).
[7] P. Gondret, M. Lance, and L. Petit, "Bouncing motion of spherical par-

ticles in fluids," Phys. Fluids **14**, 643 (2002).
[8]F.-L. Yang and M. L. Hunt, "Dynamics of particle-particle collisions in a viscous liquid," Phys. Fluids **18**, 121506 (2006).
[9]D. Legendre, C. Daniel, and P. Guiraud, "Experimental study of a drop bouncing on a wall in a liquid," Phys. Fluids **17**, 097105 (2005).
[10]D. Legendre, R. Zenit, C. Daniel, and P. Guiraud, "A note on the modelling of the bouncing of spherical drops or solid spheres on a wall in viscous fluid," Chem. Eng. Sci. **61**, 3543 (2006).
[11]H. Lamb, *Hydrodynamics* (Dover, New York, 1945).
[12]H.-K. Tsao and D. L. Koch, "Collisions of slightly deformable, high Reynolds numbers bubbles with short-range repulsive forces," Phys. Fluids **6**, 2561 (1994).
[13]H.-K. Tsao and D. L. Koch, "Observations of high Reynolds number bubbles interacting with a rigid wall," Phys. Fluids **9**, 44 (1997).
[14]K. Malysa, M. Krasowska, and M. Rrzan, "Influence of surface active substances on bubble motion and collision with various interfaces," Adv. Colloid Interface Sci. **114–115**, 205 (2005).
[15]M. Krasowska and K. Malysa, "Wetting films in attachement of the colliding bubble," Adv. Colloid Interface Sci. **134–135**, 138 (2007).
[16]J. Zawala, M. Krasowska, T. Dabros, and K. Malysa, "Influence of bubble kinetic energy on its bouncing during collisions with various materials," Can. J. Chem. Eng. **85**, 669 (2007).
[17]D. Richard and D. Quéré, "Bouncing water drops," Europhys. Lett **50**, 769 (2000).
[18]K. Okumura, F. Chevy, D. Richard, D. Quéré, and C. Clanet, "Water spring: A model for bouncing drops," Europhys. Lett. **62**, 237 (2003).
[19]F. Vincent, A. Le Goff, G. Lagubeau, and D. Quéré, "Bouncing bubbles," J. Adhes. **83**, 897 (2007).
[20]J. Magnaudet and I. Eames, "The motion of high-Reynolds-number bubbles in inhomogeneous flows," Annu. Rev. Fluid Mech. **32**, 659 (2000).
[21]D. W. Moore, "The velocity of rise of distorted gas bubbles in a liquid of small viscosity," J. Fluid Mech. **23**, 749 (1965).
[22]L. Shiller and A. Z. Nauman, "A drag coefficient correlation," Z. Ver. Dtsch. Ing. **77**, 318 (1933).
[23]P. C. Duineveld, "The rise of an ellipsoidal bubble in water at high Reynolds number," J. Fluid Mech. **292**, 325 (1995).
[24]R. Zenit and J. Magnaudet, "Path instability of rising spheroidal air bubbles: A shape-controlled process," Phys. Fluids **20**, 061702 (2008).
[25]R. H. Davis, J. M. Serayssol, and E. J. Hinch, "The elastohydrodynamic collision of two spheres," J. Fluid Mech. **163**, 479 (1986).
[26]S. Weinbaum, C. Lawrence, and Y. Kuang, "The inertial draining of a thin fluid layer between parallel plates with a constant normal force. Part 1. Analytic solutions; inviscid and small-but fnite-Reynolds-number limit," J. Fluid Mech. **156**, 463 (1985).
[27]A. H. Lefebvre, *Atomization and Sprays* (Hemisphere, New York, 1989).
[28]E. Falcon, C. Laroche, S. Fauve, and C. Coste, "Behavior of one inelastic ball bouncing repeatedly off the ground," Eur. Phys. J. B **3**, 45 (1998).